Journal of Marine Science and Technology

Volume 25 | Issue 6 Article 16

A TIME-DOMAIN NUMERICAL TOOL FOR A WAVE ENERGY ATTENUATOR WITH THE SPH METHOD

Da-Wei Chen
Institute of Ocean Energy, Saga University, 1 Honjo machi, Saga-shi, Saga, Japan. Department of System Engineering and Naval Architecture, National Taiwan Ocean University, Keelung, Taiwan, R.O.C.

Shuichi Nagata
Institute of Ocean Energy, Saga University, 1 Honjo machi, Saga-shi, Saga, Japan.

Shiaw-Yih Tzang
Department of Harbor and River Engineering, National Taiwan Ocean University, Keelung, Taiwan, R.O.C., sytzang@mail.ntou.edu.tw

Yasutaka Imai
Institute of Ocean Energy, Saga University, 1 Honjo machi, Saga-shi, Saga, Japan.

Chih-Min Hsieh
Department of Marine Information and Technology, National Kaohsiung Marine University, Kaohsiung, Taiwan, R.O.C

See next page for additional authors

Recommended Citation

Chen, Da-Wei; Nagata, Shuichi; Tzang, Shiaw-Yih; Imai, Yasutaka; Hsieh, Chih-Min; and Chen, Jiahn-Horng (2017) "A TIME-DOMAIN NUMERICAL TOOL FOR A WAVE ENERGY ATTENUATOR WITH THE SPH METHOD," *Journal of Marine Science and Technology*: Vol. 25: Iss. 6, Article 16.
DOI: 10.6119/JMST-017-1226-16
Available at: https://jmstt.ntou.edu.tw/journal/vol25/iss6/16

A TIME-DOMAIN NUMERICAL TOOL FOR A WAVE ENERGY ATTENUATOR WITH THE SPH METHOD

Authors

Da-Wei Chen, Shuichi Nagata, Shiaw-Yih Tzang, Yasutaka Imai, Chih-Min Hsieh, and Jiahn-Horng Chen

Journal of Marine Science and Technology, Vol. 25, No. 6, pp. 752-760 (2017)
DOI: 10.6119/JMST-017-1226-16

A TIME-DOMAIN NUMERICAL TOOL FOR A WAVE ENERGY ATTENUATOR WITH THE SPH METHOD

Da-Wei Chen[1, 4], Shuichi Nagata[1], Shiaw-Yih Tzang[2],
Yasutaka Imai[1], Chih-Min Hsieh[3], and Jiahn-Horng Chen[4]

Key words: wave energy attenuator, smooth particle hydrodynamics, floating object, rotating angle, energy conversion.

ABSTRACT

The wave energy attenuator is a floating device which operates perpendicular to the wave fronts and captures wave energy from the relative motions of two hinged floaters as waves passing by them. For establishing the time-domain numerical tools to evaluate the performance of a wave energy attenuator, a Smoothed Particle Hydrodynamic (SPH) model with mesh-free method was adopted to simulate the hydrodynamic behaviors of each floating object. Three different wave heights of 6 cm, 7 cm, and 10.4 cm of the same period of 1.22 s were commonly derived from typical potential oceanic zones offshore Taiwan and Japan. Comparisons of the hydrodynamic behaviors of an attenuator show that the device has an averaged rotating angles of about 9-15 degrees for the upstream floater (Floater A) and of smaller about 6-9 degrees for the downstream floater (Floater B) during an averaged wave cycle. For energy conversions, the wave height of 6 cm has the maximum capture factor of 22%, which is larger than those of 7 cm and 10.4 cm by about 4% and 17%, respectively. Moreover, the converted ratio by an attenuator WEC from wave energy loss are about 67% at H = 6 cm, 38% at H = 7 cm, and 19% at H = 10.4 cm, respectively.

I. INTRODUCTION

Among many wave energy conversion techniques in the recent decade, Pelamis is one of the well-developed wave energy convertors (WECs) with an attenuator type that absorbs energy of ocean waves to generate electricity. An attenuator WEC operates perpendicular to the wave fronts and captures wave energy from the relative motions of two hinged floaters as wave passing by them, as shown in Fig. 1. Many researches have been carried out to develop such a typical device due to its advantages as a floating attenuator WEC with flexible deployments at different water depths and wave height reductions in the rear water fields. So far, those results have given that this type of device consists of some typical properties on dynamic mechanisms. For example, Holmberg et al. (2011) reported that the length of an attenuator' floating segments should be smaller than 1/4 of the wavelength (λ) for higher performance. Moreover, the device is most suited to relatively long waves ($T_e > 7$ s) for better performance. For optimal design based on potential theory, Haren and Mei (1979) investigated that a train of three floater segments with different lengths had been proofed to be the optimal design on capture efficiency at different wave fields. Also, Zhou and Eden (2015) reported that comparisons of different segment lengths of an attenuator show that the shorter one had the higher energy-capturing performance.

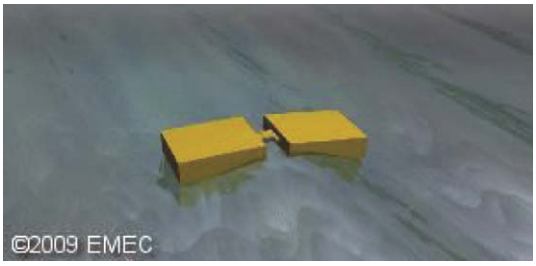

Fig. 1. Illustration of wave energy attenuator.

For evaluating the floating motions and operating efficiency, some numerical tools such as WAMIT, NEMOH, WEC-Sim with potential theory are widely used to help predicting the Response Amplitudes Oscillations (RAO) and motion properties for the WEC in the frequency and time domain. In addition, several computational Fluid Dynamics (CFD) such as OpenFOAM and Fluent are also frequently used to deal with the hydrodynamic problems in the WEC's operations. However for these numerical tools, floating motions under wave actions require usage of dynamic meshes or numerical schemes on grid background. Compared

Paper submitted 09/14/17; revised 11/02/17; accepted 11/09/17. Author for correspondence: Shiaw-Yih Tzang(e-mail: sytzang@mail.ntou.edu.tw).
[1] *Institute of Ocean Energy, Saga University, 1 Honjo machi, Saga-shi, Saga, Japan.*
[2] *Department of Harbor and River Engineering, National Taiwan Ocean University, Keelung, Taiwan, R.O.C.*
[3] *Department of Marine Information and Technology, National Kaohsiung Marine University, Kaohsiung, Taiwan, R.O.C.*
[4] *Department of System Engineering and Naval Architecture, National Taiwan Ocean University, Keelung, Taiwan, R.O.C.*

to the grid methods, a mesh-free one with Lagrangian approach may be more convenient to deal with the problem on such a floating object.

A particle method, Smoothed Particle Hydrodynamic (SPH) scheme, is originally developed for astrophysics by Lucy (1977) and Gingold and Monaghan (1977). Later, Monaghan (1994) first applied it to surface flows, including simulations of the dam breaking and the wave breaking. Recently, SPH has become more widely applied to CFD, especially on fluid-solid interactions (Bonet et al., 2004; Antoci et al., 2007; Violeau et al., 2007). For ocean energy, the SPH method had been applied to evaluate an offshore floating Oscillating Water Column WEC in the open sea by Iturrioz et al. (2014). The authors had also developed numerical tools based on SPH methods for estimating other types of the WECs, including a bottom-hinged converter (Chen et al., 2014), a sliding type converter (Chen et al., 2012) and those with Power Take-Off (PTO) system (Chang et al., 2015). In this paper, the aim is to establish a 2-D numerical model flume with SPH method for simulating the motions of a floating attenuator WEC with two floaters. Key dynamic aspects of the interactions between waves and moving attenuator's floaters shall first be highlighted from previous work. Then evaluations shall be carried out on the capture efficiency of the attenuator WEC at typical wave conditions in both Taiwan's and Japanese potential oceanic waters.

II. METHODOLOGY

1. Governing Equations

The SPH method based on the Navier-Stokes equation consisting of the continue and momentum equations, describes the motion of a viscous flow with SPH discretization formulae expressed as follows

$$\frac{d\rho}{dt} = \sum_{j=1}^{N} m_j \vec{u}_{ij} \cdot \nabla_i W_{ij} \tag{1}$$

$$\frac{d\vec{u}_i}{dt} = \sum_{j=1}^{N} m_j \left(\frac{P_i}{\rho_i^2} + \frac{P_j}{\rho_j^2} \right) \cdot \nabla_i W_{ij} + \Pi_{ij} + \vec{g} \tag{2}$$

where $\vec{u}$ denotes the vector velocity, subscript i and j the assigned number of each particle. Therefore, $\vec{u}_{ij} = \vec{u}_i - \vec{u}_j$ is the velocity variation of the particle between the velocity, W the kernel function, p the fluid pressure, m the particle mass, Π an empirical approximation of the viscosity effects by Monaghan et al. (2003). $\vec{g}$ the gravitational acceleration.

1) Equation of State

Some researchers developed the incompressible flow in SPH method using the Poisson equation ($\nabla^2 P = \rho(\nabla v / \nabla t)$), e.g., Khayyer et al. (2008) and Shao and Lo (2003). This method is commonly solved in Eulerian approach but is time-consuming for solving them. Therefore, the Tait equation by Monaghan (1994) have been adopted due to low density variations and low computational cost. It is given as

$$P = B\left[\left(\frac{\rho}{\rho_0} \right)^{\gamma} - 1 \right] \tag{3}$$

where $\gamma = 7$ a constant, $\rho_0 = 1000$ kg/m^3 the reference density, and $B = c^2 \rho_0 / \gamma$ with sound speed (c), governs the relative density fluctuation. In addition, the c is relative to the Mach number (M_a). Since the actual sound speed being very large, the corresponding Mach number is very small. Therefore, the density fluctuation could be nearly negligible, and the fluid is approached as an ideally incompressible.

2) Viscosity

The artificial viscosity developed by Monaghan (1992) has been widely used due to its simplicity. The equations are expressed as follows

$$\Pi_{ij} = \begin{cases} \dfrac{-\alpha \overline{c}_{ij} \mu_{ij}}{\overline{\rho}_{ij}} & \vec{u}_{ij} \vec{r}_{ij} < 0 \\ 0 & \vec{u}_{ij} \vec{r}_{ij} > 0 \end{cases} \tag{4}$$

with

$$\mu_{ij} = \frac{h \vec{u}_{ij} \vec{r}_{ij}}{\vec{r}_{ij}^{\,2} + \eta^2} \tag{5}$$

where the position and the velocity of particle i and j are $\vec{r}_{ij} = \vec{r}_i - \vec{r}_j$ and $\vec{u}_{ij} = \vec{u}_i - \vec{u}_j$, respectively. The averaged sound speed is $\overline{c}_{ij} = (c_i + c_j)/2$, the averaged density $\overline{\rho}_{ij} = (\rho_i + \rho_j)/2$, $\eta^2 = 0.01\, h^2$, α is an experiential parameter by Monaghan et al. (2003).

2. Fluid-Solid Interaction

1) A Floating Object

According to Monaghan et al. (2003), the force on each boundary particle is computed by summing up the contribution from all the surrounding water particles. Denoting the force per unit mass on a moving body boundary particle k by $\vec{f}_k$, as follow

$$\vec{f}_k = \sum_{k=1}^{N} m_k \frac{d\vec{u}_k}{dt} \tag{6}$$

where N is the total number of boundary particle as the floating object. $d\vec{u}_k / dt$ the acceleration exerted by water particle on

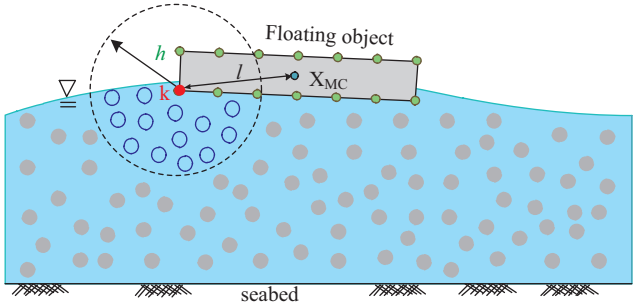

Fig. 2. Definition of floating object.

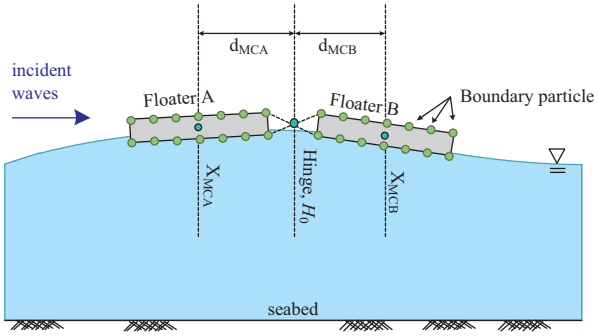

Fig. 3. Definition of wave energy attenuator with two floaters and a floating hinge.

each boundary particle, m the mass of each boundary particle. Therefore, the displacement and rotation of a floating object can be obtained from the boundary particles, the formula including the total force ($\vec{F}$) and torque ($\vec{\tau}$) can be modified as follow by Monaghan et al. (2003) and Gómez-Gesteira et al. (2010).

$$\vec{F} = \sum_{k=1}^{N} \vec{f}_k + M\vec{g} = M \cdot \frac{d\vec{v}}{dt} \tag{7}$$

$$\vec{\tau} = \sum_{j=1}^{N} l_k \cdot \vec{f}_k = I \cdot \frac{d\vec{\omega}}{dt} \tag{8}$$

where l is the distance between a boundary particle and mass center (X_{MC}) of the floating object (see Fig. 2), M and I the mass of the object and moment of inertia, respectively. Moreover, v and ω denote the moving and rotating velocities of the floating object, respectively. Note that the moving boundary forces ($\vec{f}_k$) (see Eq. (7)) contain the fluid's acting force on the floating object and the buoyancy from water particle within a smoothed radius. In particular, the SPH formulae are relative to the density so that the buoyancy of the floating object can be more easily obtained. Hence, from the total force ($\vec{F}$) and torque ($\vec{\tau}$) the moving and angular velocity of a floating object can be predicted by

$$\left(\frac{dX}{dt}\right)^{n+1} = \left(\frac{dX}{dt}\right)^{n} + \left(\frac{\vec{F}}{M}\right)^{n} \cdot \Delta t \tag{9}$$

$$\left(\frac{d\theta}{dt}\right)^{n+1} = \left(\frac{d\theta}{dt}\right)^{n} + \left(\frac{\vec{\tau}}{I}\right)^{n} \cdot \Delta t \tag{10}$$

where X and θ are the position and angular displacement, respectively. Superscript "n+1" denotes the computational value in next time step of Δt. Thus, the displacement of a floating object can be predicted by

$$(X)^{n+1} = (X)^{n} + \left(\frac{dX}{dt} + \frac{d\theta}{dt}\right)^{n} \cdot \Delta t \tag{11}$$

2) An Attenuator with Two Floaters

The targeted wave energy attenuator consists of two floaters and a floating hinge being installed on the center of between two floaters for connecting them, as show in Fig. 3. The upstream floater is denoted as Floater A, the downstream one Floater B, respectively. In general, the damping system is also installed on the floating hinge for capturing wave energy by bending under wave actions.

For an attenuator, the floating hinge (H_0) at the center as the rotating center between two floaters, the displacements and rotations based on the Eqs.(7) and (8) can be re-written as

$$\vec{F} = \vec{F}_A + \vec{F}_B = \left[\sum_{kA=1}^{N} \vec{f}_{kA} + M_A\vec{g}\right] + \left[\sum_{kB=1}^{N} \vec{f}_{kB} + M_B\vec{g}\right] \tag{12}$$

$$\vec{\tau} = \vec{\tau}_A + \vec{\tau}_B = \left[\sum_{kA=1}^{N} \left(\vec{f}_{kA} \times l_{kA}\right) - \left(M_A\vec{g} \times d_{MCA}\right)\right] + \left[\sum_{kB=1}^{N} \left(\vec{f}_{kB} \times l_{kB}\right) + \left(M_B\vec{g} \times d_{MCB}\right)\right] \tag{13}$$

where subscript A and B denote the floaters A and B, respectively. kA and kB denote the boundary particles on floater A and B. In addition, l(= $p - H_0$) denotes the distance between the boundary particle (p) to the floating hinge (H_0) in 2-D (x-z plane). Note that the torques for floater A and B due to wave acting on the floaters and their gravitational force, include different rotational directions for floater A and B from the gravity-induced body forces (see Eq. (13)). Therefore, the displacement and angular velocity of a whole attenuator system can be obtained by

$$\left(\frac{dX}{dt}\right)^{n+1} = \left(\frac{dX}{dt}\right)^{n} + \left(\frac{\vec{F}}{M_A + M_B}\right)^{n} \cdot \Delta t \tag{14}$$

$$\left(\frac{d\theta_A}{dt}\right)^{n+1} = \left(\frac{d\theta_A}{dt}\right)^{n} + \left(\frac{\vec{\tau}_A}{I_A}\right)^{n} \cdot \Delta t \tag{15}$$

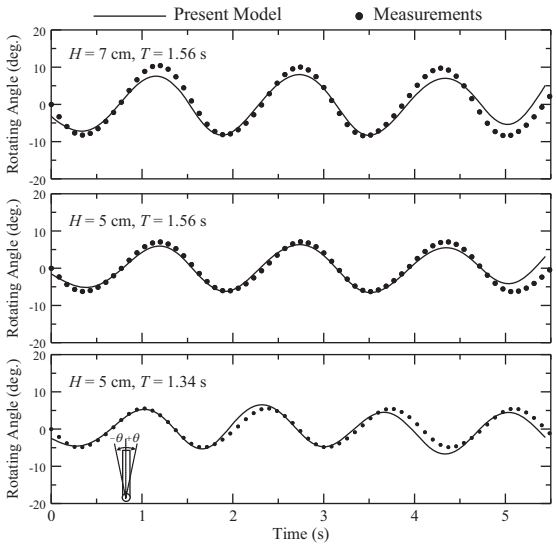

Fig. 4. Comparisons of the simulated rotating angles of a bottom-hinged wave energy converter with experimental data (Chen et al., 2014).

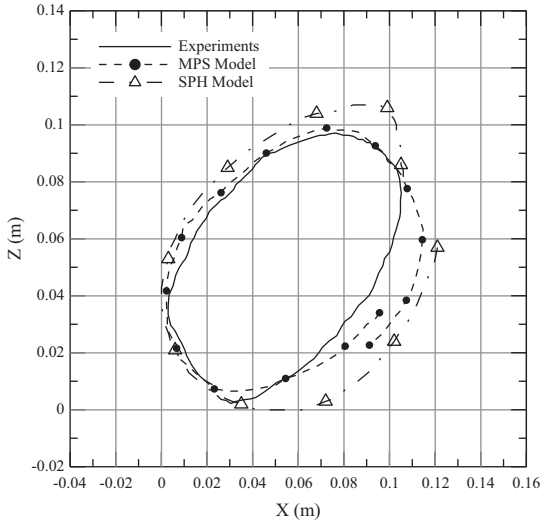

Fig. 5. Tracking the displacements of floating body by Chen et al. (2016).

$$\left(\frac{d\theta_B}{dt}\right)^{n+1} = \left(\frac{d\theta_B}{dt}\right)^{n} + \left(\frac{\vec{\tau}_B}{I_B}\right)^{n} \cdot \Delta t \tag{16}$$

Hence, the position of a floating hinge (H_0) and the mass center of floater A (X_{MCA}) and B (X_{MCB}) can be predicted by

$$(H_0)^{n+1} = (H_0)^{n} + \left(\frac{dx}{dt}\right)^{n} \cdot \Delta t \tag{17}$$

$$(X_{MCA})^{n+1} = (X_{MCA})^{n} + \left(\frac{dX}{dt} + d_{MCA} \cdot \frac{d\theta_A}{dt}\right)^{n} \cdot \Delta t \tag{18}$$

$$(X_{MCB})^{n+1} = (X_{MCB})^{n} + \left(\frac{dX}{dt} + d_{MCB} \cdot \frac{d\theta_B}{dt}\right)^{n} \cdot \Delta t \tag{19}$$

Moreover, the position of each boundary particle on the floater A (X_{KA}) and B (X_{KB}) can be predicted by

$$(X_{kA})^{n+1} = (X_{kA})^{n} + \left(\frac{dX}{dt} + l_{kA} \cdot \frac{d\theta_A}{dt}\right)^{n} \cdot \Delta t \tag{20}$$

$$(X_{kB})^{n+1} = (X_{kB})^{n} + \left(\frac{dX}{dt} + l_{kB} \cdot \frac{d\theta_B}{dt}\right)^{n} \cdot \Delta t \tag{21}$$

3. Model Highlights on Key Aspects

In order to reasonably simulate the interactions between an attenuator and waves by present SPH tool, key aspects on hinge motions, floater displacements, and a wave traveling are further highlighted. First two aspects will be based on previous work in Chen et al. (2014) and Chen et al. (2016), respectively.

1) Hinge and Floater Kinematics

For describing hinge motions, Fig. 4 (from Chen et al., 2014) shows the rotations of an bottom-hinged oscillating wave surge converter (OWSC) under different wave conditions. A rigid acrylic flap with a height of 50 cm, a thickness of 0.5 cm and a density of 1.18 kg/m^3 was driven by wave loadings. The resulting rotating angles could be reasonable simulated with high correlations of 0.96-0.99 and low variations of 0.82-1.67.

For a moored floater, Fig. 5 shows that a rigid floater with a height of 5 cm, a length of 8 cm and a density of 0.25 g/m^3 in the wave tank of 45 cm depth could be reasonably simulated for its with high correlations with experimental data (Shigemura et al., 1987) and Moving Particle Semi-implicit (MPS) method (Ikari and Gotoh, 2009).

2) Wave Decay by Viscos Effect

Waves with viscosity effects traveling through motions of an attenuator WEC is one of vital issues in a numerical tank. A solitary wave was adopted for further validating present study. According to Keulegan (1978), the formula for wave attenuation of a solitary wave in viscos flows is expressed as

$$\left(\frac{H}{d}\right)^{\frac{1}{4}} = \left(\frac{H_i}{d}\right)^{\frac{1}{4}} + \frac{1}{12}\left(1+\frac{2d}{B}\right)\sqrt{\frac{\mu}{g^{1/2}d^{2/3}}} \cdot \frac{x}{d} \tag{22}$$

where H_i is the incident wave, d the water depth, B the width of wave tank (B = 1 for 2-D tank), μ the dynamic viscosity (= 1×10^{-6} N · s/m^2). And the Keulegan's formula has been modified by Mei (1989) using perturbation method, the formula was re-written as follows

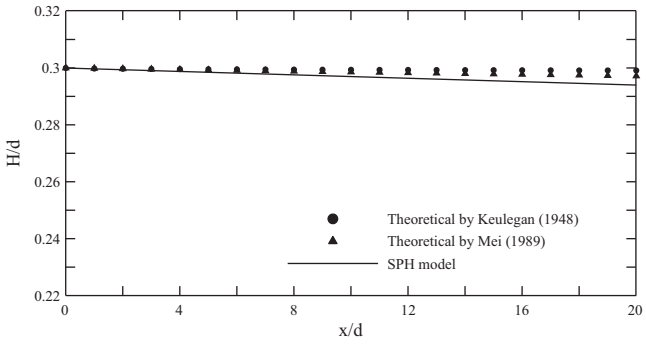

Fig. 6. Variation of dimensionless distance (x/d) with water surface elevations (H/d).

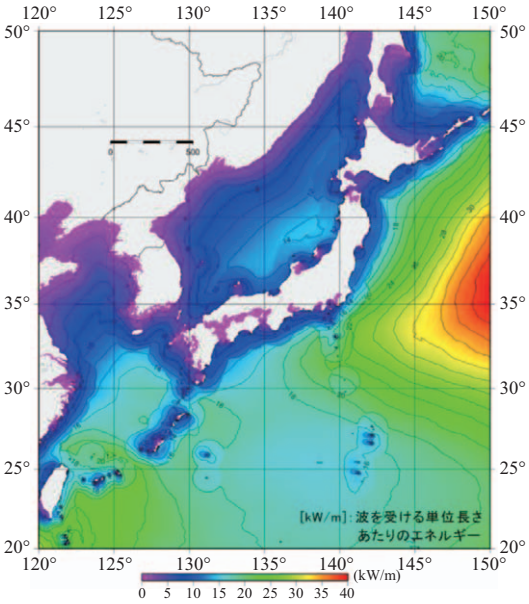

(a) The annual averaged potential distributions of wave powerin northeastern Asia by analyzingfrom field-measured data (NEDO, 2011).

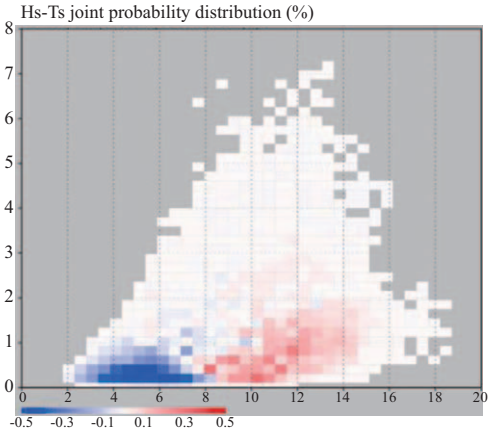

(b) data in East coasts of central Japanduring1980-2009 (Sasaki, 2012). (The red and blue colors denote the increasing and de-creasing values.)

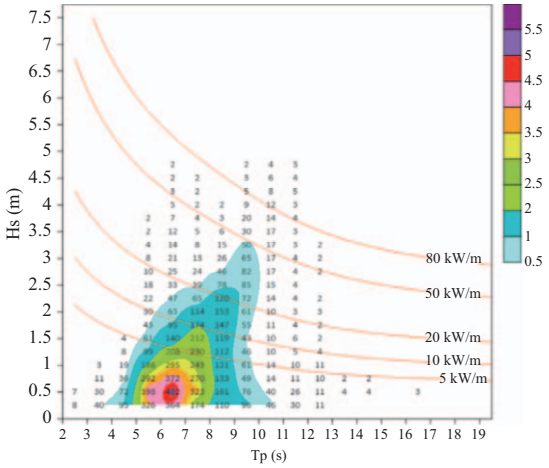

(c) Measured data in Northeastern Taiwan during 2001-2014 (Port of Keelung). (The colors denote the occurring probability.)

Fig. 7. The joint distributions of significant wave heights and wave periods in northeastern Asia.

Table 1. The wave conditions and ratio of device length and wave length.

ID	Wave height	Wave period	Wave length	Wave steepness	Device length/wave length
	H (cm)	T (s)	λ (m)	H/λ	L/λ
1	6.0	1.22	2.04	0.030	0.25
2	7.0	1.22	2.04	0.035	0.25
3	10.4	1.22	2.04	0.050	0.25

$$(H)^{\frac{1}{4}} = (H)^{\frac{1}{4}} + 0.08356\sqrt{\frac{\mu}{g^{1/2}d^2}} \cdot \frac{x}{d} \qquad (23)$$

Comparing the simulated wave attenuations with those two theoretical analyses as a solitary wave traveling in the numerical tank has the lower variations under 0.02% even for a distance $x/d >= 20$, as shown in Fig. 6. Therefore, the simulations in wave attenuation are in good agreement with the theoretical analyses implying the occurrences of wave attenuation in the downstream vicinity of an attenuator WEC should be mainly due to floaters' absorption from waves.

III. MOTIONS OF AN ATTENUATOR

1. Natural Wave Conditions Offshore Taiwan and Japan

NEDO (2011) reported that the annual averaged wave power in northeastern Asia is about 10-15 kW/m from field-measured data during 1948-2008, as shown in Fig. 7(a). It shows that the higher potential wave-power areas are far from the coastal to be in deep water. From field-measurements it is known that at some shallow water sites and during specific seasons, there could still be oceanic zones with higher wave power. For example, the northeastern Taiwan, and east coasts of central Japan and so on. Thus, long-term data from stations at both sites were adopted for analyses.

The joint distributions of significant wave heights and significant/peak wave periods in Japan and Taiwan for over 10 years are shown in Fig. 7(b) and (c). It is noted in both figures that the wave conditions ranged about 0.5-7.0 m on wave heights and 2-14 s on wave periods offshore east Japan, and about 0.5-3.5 m on wave heights and 4-10 s on wave periods offshore northeastern Taiwan. It indicates that waves in the two oceanic areas are of similar heights but of longer wave periods in areas at higher latitude than at lower one.

In order to estimate applicability of this attenuator at different wave conditions, wave heights of 1.5 m, 1.75 m, and 2.5 m with the wave period of 6.0 s for about wave power of 6.75-18.75 kW/m were adopted. For further validations on numerically simulated floater kinematics by comparing with lab-flume experiments with a water depth of 50 cm, a model scale of 1:25 were calculated. Therefore, the corresponding input wave conditions became 6 cm, 7 cm and 10 cm of heights and 1.22 s of the same period.

2. Numerical Settings

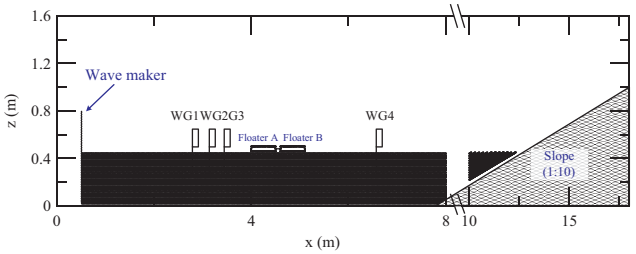

Fig. 8. A 2-D numerical tank for simulating a wave energy attenuator.

Taking into account of computational costs in simulation, the SPH method in 2-D was adopted for evaluations with negligible diffraction and refraction effects. The adopted numerical wave flume was equipped with a length of about 20 m and a depth of 0.5 m. A piston-type wave-maker was set on the upstream and a 1:10 slope on the downstream boundary for reducing reflected waves. The simulations adopted a particle spacing of ($dx = dz$) 0.02 m, and empirical coefficient (α) of 0.05 for viscosity term by Monaghan et al. (2003). For further estimating the energy attenuation, three wave gauges were installed at x = 3.4 m, 3.6 m, and 3.8 m for analyzing the reflection and at x = 6.5 m for transmissions, as shown in Fig. 8. In order to compare the variations of wave energy during wave energy attenuator being operating, incident waves with heights of 6 cm, 7 cm and 10 cm and with a period of 1.22 s were applied for a model scale of 1:25 with the same ratio of device length (L) and wave length (λ) of 0.25, as shown in Table 1. Moreover, the same length of 0.5 m for both floaters was adopted in this study. The initial settings of the model assigned 3,789 particles on the boundary, 110 particles on the floating object, and 12,202 particles in the fluid.

3. Motions with Free Surface

The motions of attenuator at different phases in the wave conditions (H = 5 cm, T = 1.22 s) are shown in Fig. 9. When wave crest approaches the attenuator, the upstream floater generates clockwise rotations, as shown in Fig. 9(a). Then Floater A transfers counter-clockwise rotation as wave crests passing it and approaching the hinge. Meanwhile, both floaters move upwards with free surface, as shown in Fig. 9(b). Both floaters continuously generate counter-clockwise rotations by the following wave trough being lower under the water surface, as shown in Fig. 9(c). As the following incident waves approaching, both floaters could be driven to be through the same motions in a wave cycle.

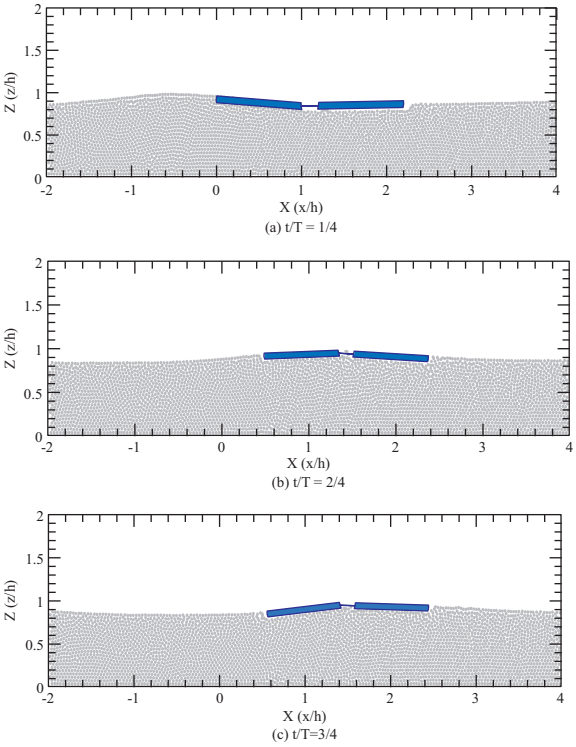

Fig. 9. The motions of the wave energy attenuator at different phases.

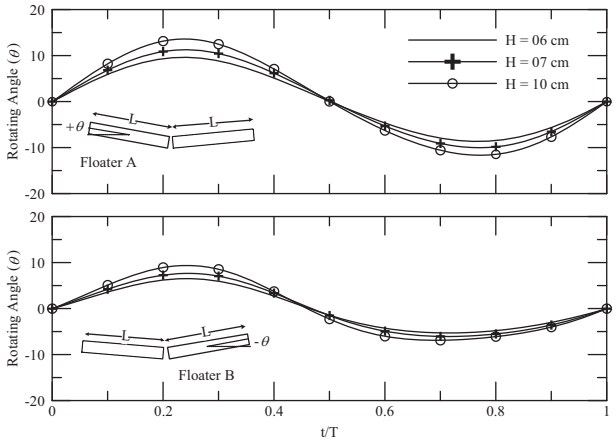

Fig. 10. Comparisons of the rotating angles of floater A and B with the same device lengths and masses. ($L_A = L_B$, $M_A = M_B$)

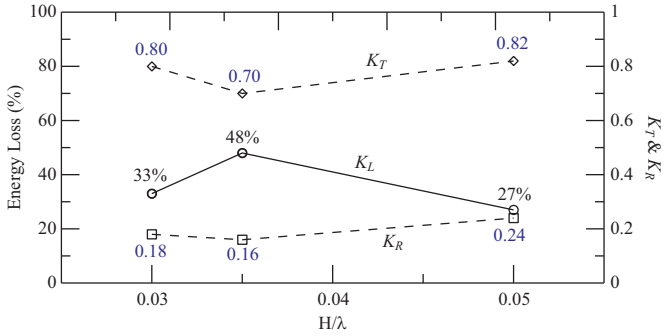

Fig. 11. Comparisons of the reflection coefficient, transmission, and energy loss.

As a result, averaged rotating angles for a wave period with different wave conditions between Floater A and Floater B are shown in Fig. 10. The positive degrees ($+\theta$) denote the rotations by counter-clockwise and the negative ones ($-\theta$) clockwise. The averaged rotating angles for maximum and minimum ones of Floater A are about 9.1° for H of 6 cm, about 10.6° for H of 7 cm, and about 14.5° for H of 10 cm. Moreover, those for the Flap B are about 6.0° for H of 6 cm, about 7.0° for H of 7 cm, and about 9.2° for H of 10 cm. The results show that Floater A at upstream tends to rotate with larger angles than Floater B at downstream. Moreover, higher incident waves could induce larger rotating angles of the floaters.

4. Evaluations on Energy Conversion

1) Wave Energy Loss at the WEC

To estimate the efficiency of a attenuator, the energy loss at the attenuator WEC with the same water depth in the numerical flume consisting of the transmission ($K_T = H_T/H_i$) and reflection coefficient (K_R), Mansard and Funke (1980) gave as

$$K_L = 1 - K_T^2 - K_R^2 \tag{24}$$

where H_i and H_T are the incident waves by gauge-3 (WG3) and transmitted waves by gauge-4 (WG4), respectively. The reflection coefficients are analyzed accordingly to Mansard and Funke (1987) from three wave gauges in front of the attenuator. For the energy conservations, the energy loss is related to the conversion of an attenuator when the incident waves passing over the device. Comparisons of the energy loss with those reflection coefficient and transmission are shown in Fig. 11. For three different incident waves, the reflection coefficients H_R were seen to be slightly larger at the highest wave steepness. At lowest and highest wave steepness of 0.030 and 0.050, transmission coefficients H_T became similarly 0.8 and 0.82, but became lowest to be 0.7 at wave steepness of 0.035 due to highest energy loss of 48 %. It suggests that transmitted waves than reflected waves be more closely dependent on the energy loss by an attenuator.

2) Captured Factor

In order to further understand the mechanical power by the attenuator, the instantaneous power $|P|$ during a wave cycle could be estimated by the expression as

$$|P| = \frac{1}{T}\int_0^T \tau(t)\omega(t)dt \tag{25}$$

where T denotes the wave period, τ the instantaneous torque by present model calculation, ω the instantaneous angular velocity. Therefore, as incident waves passing the attenuator, Floater A at the upstream and Floater B at the downstream can generate

Table 2. Averaged mechanical power by rotation of two floaters.

Floater	$\bar{\omega}$ (rad/s)	$\bar{\tau}$ (N-m)	T (s)	$\lvert\overline{P}\rvert$ (Watt/m)	$\lvert\overline{P_T}\rvert$ (Watt/m)
H = 6.0 cm					
A	0.534	1.395	1.22	0.91	1.11
B	0.333	0.504	1.22	0.20	
H = 7.0 cm					
A	0.604	1.368	1.22	1.01	1.23
B	0.325	0.566	1.22	0.22	
H = 10.2 cm					
A	0.806	0.699	1.22	0.69	0.80
B	0.505	0.179	1.22	0.11	

mechanical power by wave-induced rotations, respectively. The averaged mechanical power by attenuator operations is shown in Table 2.

It is clearly seen that both averaged angular velocity ($\bar{\omega}$) of two floaters and their variations ($\bar{\omega}_{Floator\ A} - \bar{\omega}_{Floator\ B} = 0.201$ for H of 6 cm, 0.279 for H of 7 cm, and 0.301 for H of 10 cm) between floaters gradually increased with increasing wave heights. In additions, the averaged torques ($\bar{\tau}$) for upstream Floater A were larger than that for downstream Floater B. For energy conversions, the averaged total mechanical power $\overline{P_T}$ with 1.22 Watt at H of 7 cm is the largest than the 1.11 for H of 6 cm and 0.80 for H of 10 cm. By comparing the wave energy loss in Fig. 11 and captured power in Table 2 suggest that the highest wave energy could be captured in conditions with the lowest wave reflections and transmissions, respectively. That is the highest wave energy loss and captured mechanical power for H/L = 0.035 were highly related to lowest wave reflections and transmissions with 0.16 and 0.70, respectively. Moreover, for an attenuator WEC higher reflections are directly related to higher transmissions resulting in lower energy losses and even lower mechanical power.

According to theoretical analyses by Dean and Dalrymple (1991), the theoretical wave power ($\lvert\overline{P_i}\rvert$) from the average energy flux for regular waves can be evaluated by

$$\begin{aligned}\left|\overline{P_i}\right| &= E \cdot Cn \\ &= \frac{1}{8}\rho g H^2 \cdot c \cdot \left[\frac{1}{2}\left(1+\frac{2kh}{\sinh(2kh)}\right)\right]\end{aligned} \tag{26}$$

where E is the total energy by summing up kinetic energy and potential energy, Cn the speed of energy transmission, c the wave speed. Therefore, the theoretical wave power are obtained 4.95 Watt for H = 6 cm, 6.73 Watt for H = 7cm, and 14.87 Watt for H = 10 cm, respectively. Comparisons of the captured factors (*CFs*) of an attenuator WEC show that the *CF* of 22% for H = 6 cm is the highest value than that of 18 % for H = 7 cm and 5% for H = 10 cm, respectively, as shown in Table 3.

Table 3. Captured factors of an attenuator WEC from theoretical incident wave power and mechanical power.

ID	H (cm)	$\lvert\overline{P_T}\rvert$ (Watt/m)	$\lvert\overline{P_i}\rvert$ (Watt/m)	CF ($\lvert\overline{P_T}\rvert/\lvert\overline{P_i}\rvert$) (%)
1	6.0	1.11	4.95	22
2	7.0	1.23	6.73	18
3	10.4	0.80	14.87	5

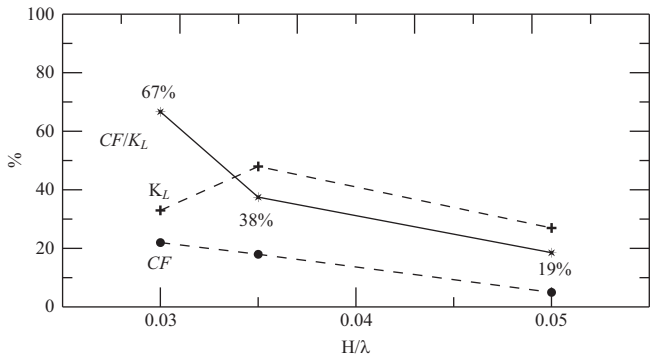

Fig. 12. Comparisons of the energy loss, captured factors, and real converted ratio by an attenuator WEC.

As incident waves passing by an attenuator WEC, K_L and *CF* are the key index to estimate the energy loss of waves and energy conversions of a device, respectively. By comparing K_L and *CF* find that the highest $\lvert\overline{P_i}\rvert$ at H = 10.4 cm does not necessarily have a highest *CF*, also the highest K_L and $\lvert\overline{P_T}\rvert$ at H = 7 cm do not either have a highest *CF*. Hence, the real converted ratio (K_L/CF) by an attenuator WEC from the wave energy loss are about 67% at H = 6 cm, 38% at H = 7 cm, and 19% at H = 10.4 cm, respectively, as shown in Fig. 12.

IV. CONCLUSIONS

The time domain mathematical model of a floating attenuator WEC with two floaters in a SPH 2-D numerical wave flume has been developed for estimating the wave-induced hydrodynamic behaviors. Based on previous developed schemes including a fixed hinge rotations and a floater motions and current wave decay by viscos effect testing show that the simulations by present model could obtain the reasonable results between the theoretical and experimental data.

The hydrodynamic behaviors were further investigated on rotating angles of an attenuator WEC with regular wave trains of 6 cm, 7 cm and 10.4 cm in height and 1.2 s in period, which are commonly derived from potential oceanic areas offshore Taiwan and Japan. For the simulations, the attenuator has averaged rotating angles of about 9-15 degrees for upstream Floater A at and about 6-9 degrees for downstream Floater B during a wave cycle. For energy conversions, Floater A at the upstream could generate higher averaged angular velocity ($\overline{\omega}$) and averaged torque ($\overline{\tau}$) than Floater B at the downstream. Therefore, the mechanical power for Floater A resulted in an averaged 0.87 Watt higher than that for Floater B by averaged 0.18 Watt. Moreover, the attenuator at wave steepness of 0.034 had the maximum energy loss of about 48% and maximum mechanical power 1.23 Watt higher than others by 15-21% on energy loss and by 10-35% on mechanical power, respectively. However, estimating the *CF*s from incident wave power further illustrates that the wave height of 6 cm has the maximum *CF* by 22%, which is larger than that of 7 cm and 10.4 cm by about 4% and 17%, respectively. Moreover, under a fixed *T*, the *H* of 10.4 cm with the highest incident wave power could drive the largest motions of an attenuator WEC than others, but it does not necessarily have a highest *CF*. Also the highest *KL* and $\left|\overline{P_T}\right|$ at *H* of 7 cm do not either have a highest *CF*. Overall, the real converted ratio by an attenuator WEC from the wave energy loss are about 67% at $H = 6$ cm, 38% at $H = 7$ cm, and 19% at $H = 10.4$ cm, respectively.

In future work, experimental results shall further be carried to evaluate the optimal design for an attenuator WEC with power take-off system and different floater lengths by present model.

REFERENCES

Antoci, C., M. Gallati and S. Sibilla (2007). Numerical Simulation of Fluid-Structure Interaction by Sph. 4th MIT Conference on Computational Fluid and Solid Mechanics, Cambridge, MA, 879-890.

Bonet, J., S. Kulasegaram, M. X. Rodriguez-Paz and M. Profit (2004). Variational formulation for the smooth particle hydrodynamics (SPH) simulation of fluid and solid problems. Computer Methods in Applied Mechanics and Engineering 193(12-14), 1245-1256.

Chang, Y.-C., D.-W. Chen, Y.-C. Chow, S.-Y. Tzang, C.-C. Lin and J.-H. Chen (2015). Theoretical analysis and SPH simulation for the wave energy captured by a bottom-hinged OWSC. J. Mar. Sci. Technol.-Taiwan 23(6), 901-908.

Chen, D.-W., S. Nagata and Y. Imai (2016). Modelling wave-induced motions of a floating wec with mooring lines using the SPH method. The Asian Wave and Tidal Energy Conference (AWTEC), Singapore, 449-454.

Chen, D.-W., S.-Y. Tzang, C.-M. Hsieh, Y.-C. Chow, J.-H. Chen, C.-C. Lin and R. R. Hwang (2014). Numerical modeling of wave-induced rotations of a bottom-hinged flapper with a SPH model. J. Mar. Sci. Technol.-Taiwan 22(3), 372-380.

Chen, D.-W., N.-Y. Zeng, C.-M. Hsieh, S.-Y. Tzang, J.-H. Chen and R. R. Hwang (2012). Modeling wave-induced motions of a sliding flapper with the SPH method, Chinese-German Joint Symposium on Coastal and Ocean Engineering, Keelung, Taiwan, 583-588.

Dean, R. G. and R. A. Dalrymple (1991). Water Wave Mechanics for Engineers and Scientists. World Scientific.

Gómez-Gesteira, M., B. D. Rogers, R. A. Dalrymple, A. J. C. Crespo and M. Narayanaswamy (2010). User Guide for the Sphysics Code V2.0. http://wiki.manchester.ac.uk/sphysics.

Gingold, R. A. and J. J. Monaghan (1977). Smoothed particle hydrodynamics - theory and application to non-spherical stars. Mon. Not. Roy. Astron. Soc. 181375-389.

Haren, P. and C. C. Mei (1979). Wave power extraction by a train of rafts: hydrodynamic theory and optimum design. Applied Ocean Research 1(3), 147-157.

Holmberg, P., M. Andersson, B. Bolund and K. Strandanger (2011). Wave power, surveillance study of the development. Elforsk rapport 11:02, 47.

Ikari, H. and H. Gotoh (2009). Lagrangian particle method for tracking of buoy moored by chain. Proceedings of the Nineteenth International Offshore and Polar Engineering Conference (ISOPE 2009), Osaka, Japan, 371-375.

Iturrioz, A., R. Guanche, J. A. Armesto, M. A. Alves, C. Vidal and I. J. Losada (2014). Time-domain modeling of a fixed detached oscillating water column towards a floating multi-chamber device. Ocean Engineering 7665-74.

Keulegan, G. H. (1978). Gradual damping of solitary wave. J. Res. Natl. Bur. Stand 40(6), 487-498.

Khayyer, A., H. Gotoh and S. D. Shao (2008). Corrected incompressible SPH method for accurate water-surface tracking in breaking waves. Coastal Engineering 55(3), 236-250.

Lucy, L. B. (1977). Numerical approach to the testing of the fission hypothesis. Astron. J. 82(12), 1013-1024.

Mansard, E. P. D. and E. R. Funke (1980). The measurement of incident and reflected spectra using a least squares method. Proceeding of the 17th International Conference on Coastal Engineering, 154-172.

Mansard, E. P. D. and E. R. Funke (1987). On the Reflection Analysis of Irregular Waves, 38.

Mei, C. C. (1989). The Applied Dynamics of Ocean Surface Waves. World Scientific.

Monaghan, J. J. (1992). Smoothed particle hydrodynamics. Annual Review of Astronomy and Astrophysics 30(1), 543-574.

Monaghan, J. J. (1994). Simulating free surface flows with SPH. Journal of Computational Physics 110(2), 399-406.

Monaghan, J. J., A. Kos and N. Issa (2003). Fluid motion generated by impact. Journal of Waterway Port Coastal and Ocean Engineering-Asce 129(6), 250-259.

NEDO (2011). Proposal for Ocean Energy Potential Working, 365. (In Japanese)

Sasaki, W. (2012). Changes in wave energy resources around Japan. Geophysical Research Letters 39(23), L23702.

Shao, S. and E. Y. M. Lo (2003). Incompressible SPH method for simulating newtonian and non-newtonian flows with a free surface. Advances in Water Resources 26(7), 787-800.

Shigemura, T., K. Hayashi and T. Kouzaki (1987). Dynamic behavior of a mooring buoy subject to Rough Seas. 621-625. (in Japanese)

Violeau, D., C. Buvat, K. Abed-Meraim and E. de Nanteuil (2007). Numerical modelling of boom and oil spill with SPH. Coastal Engineering 54(12), 895-913.

Zhou, D. and J. A. Eden (2015). Optimal design of a multibody self-referencing attenuator. Journal of Power and Energy Engineering 359-369.